AUTONOMOUS AND CONTINUOUS GEORECTIFICATION OF MULTI-ANGLE IMAGING SPECTRO-RADIOMETER (MISR) IMAGERY

Veljko M. Jovanovic, Michael M. Smyth, and Jia Zong
Jet Propulsion Laboratory
Mail Stop 169-314
4800 Oak Grove Drive
Pasadena, CA 91109 USA

ABSTRACT:

A theoretical concept underlying the design of the science data processing system responsible for the autonomous and continuous georectification of multi-angle imagery is the subject of this paper. The algorithm is focused on a first time attempt to rectify and map project remotely sensed data on-line, as it comes from the instrument. The algorithm deals with the following issues: a) removal of the errors introduced by inaccurate navigation and attitude data, b) removal of the distortions introduced by surface topography, c) achieving a balance between limited hardware resources, huge data volume and processing requirements, autonomous and non-stop aspects of the production system. The key elements of the algorithm are: a) photogrammetric image point intersection, b) image matching, c) adaptive image-to-image transformation and d) ancillary (input) dataset.

1. INTRODUCTION

The Multi-Angle Imaging Spectro-Radiometer (MISR) is part of an Earth Observing System (EOS) payload to be launched in 1998 (Diner, 1991). The purpose of MISR is to study the ecology and climate of the Earth through the acquisition of systematic, global multi-angle imagery in reflected sunlight. In order to derive geophysical parameters such as aerosol optical depth, bidirectional reflectance factor, and hemispheric reflectance, measured incident radiances from the multi-camera instrument must be coregistered. Furthermore, the coregistered image data must be geolocated in order to meet experiment objectives such as: a) produce a data set of value to long-term monitoring programs and allow intercomparassions of data on time scales exceeding that of an individual satellite, and b) provide Earth Observing System (EOS) synergism, and allow data exchange between EOS-platform instruments.

In order to provide coregistered and geolocated data, the ground data processing system is designed to geometrically process multi-angle multispectral data, so that they all conform to a common map projection. This is the first time attempt to rectify and map project remotely sensed data on-line, as it comes from the instrument. We define this segment of continuous and autonomous ground processing as "georectification", and the derived product as the Georectified Radiance Product. There are two basic parameters of the Georectified Radiance Product depending on the definition of the reflecting surface: a) ellipsoid-projected radiance, and b) terrain-projected radiance. The ellipsoid-projected radiance is referenced to the surface of the WGS84 ellipsoid (no terrain elevation included) and the terrain-projected radiance is referenced to the same datum including a DEM over land and inland water.

This paper describes the theoretical concepts underlying the algorithm responsible for the georectification and production of the terrain-projected radiance product. This processing segment must remove the distortion introduced by the topography that occurs when imaging with multiple viewing angles. In addition, this is the only processing step which will directly deal with the errors in the supplied spacecraft ephemeris and attitude data. In particular, we describe the geometry of the MISR imaging event and the characteristics of the terrain-projected radiance product. Then we present a description of the algorithm used and discuss the simulated input data and prototype test results.

2. GEOMETRY OF THE MISR IMAGING EVENT

In 1998, MISR will be launched aboard the EOS AM-1 spacecraft. The baseline orbit has been selected by the EOS project to be sun-synchronous, with an inclination of $98.186°$. The orbit period of 98.88 min. and orbit precession rate of $0.986°$/day imply a ground repeat cycle of the spacecraft nadir point of 16 days. This orbit is referred to as the "705 km" orbit, although the actual altitude varies from about 704 km to a maximum of 730 km. The orbit will have an equatorial crossing time of 10:30 a.m.

The MISR instrument consists of nine push-broom cameras. The cameras are arranged with one camera pointing toward the nadir (designated An), one bank of four cameras pointing in the forward direction (designated Af, Bf, Cf, and Df in order of increasing off-nadir angle), and one bank of four cameras pointing in the aftward direction (using the same convention but designated Aa, Ba, Ca, and Da). Images are acquired with nominal view angles, relative to the surface reference ellipsoid, of $0°$, $±26.1°$, $±45.6°$, $±60.0°$, and $±70.5°$ for An, Af/Aa, Bf/Ba, Cf/Ca, and Df/Da, respectively. The instantaneous displacement in the along-track direction between the Df and Da views is about 2800 km (see Figure 1). Each camera uses four Charge-Coupled Device (CCD)

176

International Archives of Photogrammetry and Remote Sensing. Vol. XXXI, Part B2. Vienna 1996

line arrays in a single focal plane. The line arrays consist of 1504 photoactive pixels plus 16 light-shielded pixels per array, each 21 μm x 18 μm. Each line array is filtered to provide one of four MISR spectral bands. The spectral band shapes will nominally be Gaussian, and centered at 443, 555, 670, and 865 nm. Because of the physical displacement of the four line arrays within the focal plane of each camera, there is an along track displacement in the Earth views at the four spectral bands. This must be corrected for within ground data processing. The cross-track instantaneous field of view (IFOV) and sample spacing of each pixel is 275 m for all of the off-nadir cameras, and 250 m for the nadir camera. Along-track IFOV's depend on view angle, ranging from 250 m in the nadir to 707 m at the most oblique
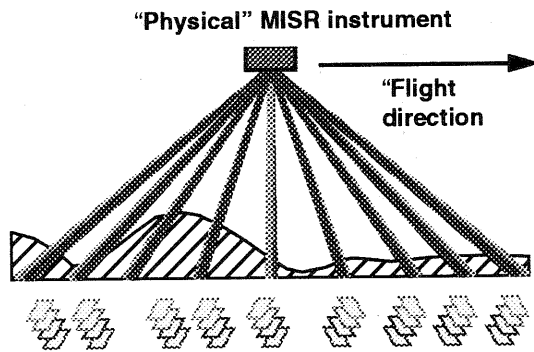
takes about seven minutes for any single location along this track to be observed by the nine MISR cameras. The science objectives require this set of multi-angle images to be geolocated and coregistered, in order for the higher-level geophysical retrievals to occur. Furthermore, within any single camera, the images in the four MISR spectral bands are slightly displaced in the along-track direction, as a consequence of the instrument design. Therefore, ground data processing must also compensate for this, by effecting a superposition of the multi-spectral data.

In an abstract world the terrain-projected radiance product may be looked upon as the data collected by a "virtual" MISR (see Figure 2.)
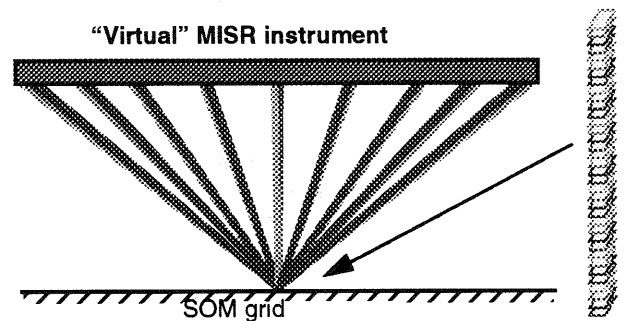

"Physical" MISR instrument

"Flight direction

Figure 1: MISR imaging event

"Virtual" MISR instrument

SOM grid

Figure 2: Terrain-projected radiance product: output from a "virtual" MISR.

angle. Sample spacing in the along-track direction is 275 m in all cameras.

In order to find the geolocation corresponding to the pixel's field of view, the pixel pointing direction is expressed in the Geocentric coordinates system, as follows:

$$\hat{\rho} = T_1 T_2 \hat{r} \qquad (1)$$

where $\hat{r}$ is the pixel pointing direction relative to the instrument coordinate system defined by the observable image coordinates and the set of constants representing the instrument interior orientation parameters. T_2 represents the transformation between the instrument and spacecraft coordinate axes. T_1, defined by the ephemeris and attitude data at the time of imaging, represents the transformation between the spacecraft and Geocentric coordinate system. Equation (1) is an often used photogrammetric model suitable for various image-ground point determinations required for satellite based imagery.

3. TERRAIN-PROJECTED RADIANCE PRODUCT

As described in the previous section the MISR instrument acquires, at any given time, push-broom imagery from nine widely separated locations along the sub-spacecraft track. It

Effectively, this product represents collection of about 140 x 9 digital image maps of the entire globe, over land and inland water, obtained during a period of 6 years. Each digital map contains radiances from four spectral bands. We have selected Space Oblique Mercator (Snyder, 1987) as the reference map projection grid, because it is design to be suitable for continuous mapping of satellite imagery. The ground resolution of the map grid is 275 m.

The spatial horizontal accuracy goal associated with these maps and requested by the science algorithms, is an uncertainty better then ±275 m at a confidence level of 95%. Obviously this kind of accuracy requires knowledge of a DEM and removal of the displacement due to relief. In addition, the accuracy specifications for the supplied spacecraft navigation and attitude data suggest the possibility of horizontal errors of about 2 km in the most oblique cameras. The next section discusses the algorithm which accounts for the displacement due to the topography and errors in the spacecraft data prior to the resampling of the acquired MISR imagery to the map grid.

4. GEORECTIFICATION ALGORITHM

4.1 Overview

In addition to the spatial accuracy requirements, the georec-

177

International Archives of Photogrammetry and Remote Sensing. Vol. XXXI, Part B2. Vienna 1996

tification algorithm must allow for the design of the process-ing system which satisfies the following criteria:
a) Balance between limited hardware resources, huge data volume and processing requirements.
b) Autonomous and non-stop production throughout the mis-sion.

Consequently, the adopted processing scenario must meet objectives, such as:

1. Reduce processing through the use of specialized input dataset.
2. Provide the best possible input for the automatic image matching required to remove errors from the supplied spacecraft navigation and attitude data.
3. Have an adaptive processing schema with regards to the magnitude of navigation and attitude data. Large errors require more processing.
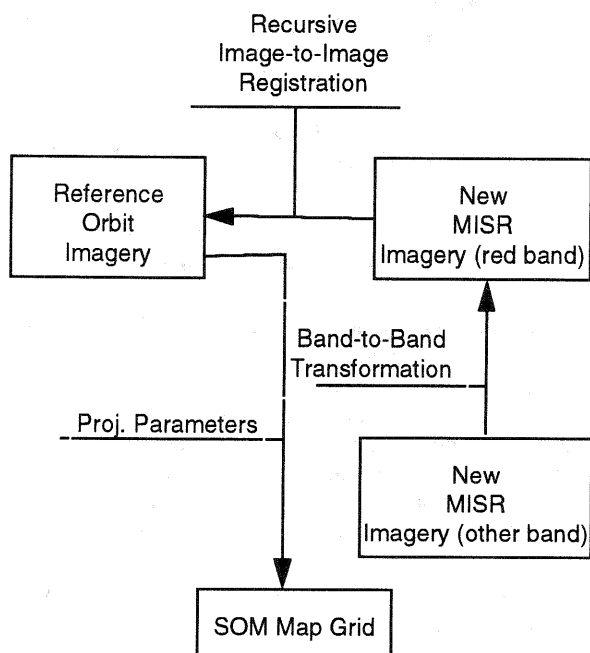
**Recursive
Image-to-Image
Registration**

Figure 3: Georectification Overview

In the approach to meet the above objectives we make use of ancillary datasets, a) a set of Projection Parameters (PP) and b) Reference Orbit Imagery (ROI), produced at the beginning of the mission. The major information indirectly contained in these datasets are error free navigation and attitude data, georeference, and surface topography relative to the various geometries of the nine MISR cameras. This information is routinely exploited through a hybrid image registration algorithm. In particular, the autonomous and continuous georectification is reduced to an image registra-tion between ROI and new MISR imagery which consists of

the following elements:

a) Image Point Intersection (IPI): a backward projection function used to provide an initial location of the conju-gate points (Paderes, 1989).
b) Image matching for the precise identification of the conjugate points.
c) Transformation (mapping) function between two images.

The registration method is adaptive with regard to the char-acter and size of misregistration, in order to minimize the size of the processing load. The adaptive nature of the algo-rithm is attained by recursively dividing images into subre-gions until the required registration accuracy is achieved. Initially, due to the push-broom nature of the MISR cameras, subregions are rectangles extending over the image in the cross-track direction. The mapping function associated with a subregion is a modification of the affine transform which includes known geometric characteristics of the MISR imag-ing event. Once the mapping between the two images is established, the last processing step is the assignment of the appropriate radiance value to the grid point of the SOM map. This is done by one of the standard (e.g. bilinear) resa-mpling methods.
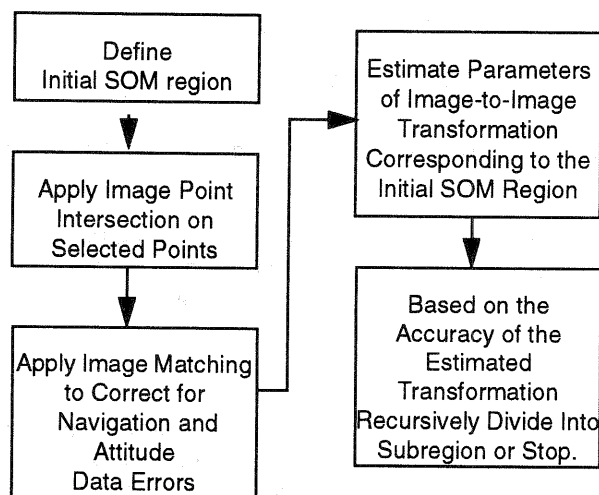

Figure 4: Recursive Image-to-Image Registration

Additional techniques are required so that autonomous pro-duction runs are unaffected by the less than perfect input data. Some of the more obvious examples are the presence of cloudy regions, water bodies, and deserts. These types of conditions significantly reduce the number of conjugate points available to determine the transformation function. In such cases additional techniques must be implemented. In some cases, searching for cloud-free land in the local neigh-borhood may be sufficient. In other cases, where a large region of data is without conjugate points, use of information obtained through the registration of the closest subregion is

178

International Archives of Photogrammetry and Remote Sensing. Vol. XXXI, Part B2. Vienna 1996

applied. The idea is to correct for slowly varying parameters through the use of a Kalman filter built while processing previous subregions.

Also included in the algorithm is a blunder detection technique aimed at removing possible blunders coming from the image matching. This utilizes statistic results obtained from the least-square estimation of the transformation function.

4.2 Creation of ancillary (input) dataset

The creation of the ancillary dataset in the first several months of the mission is directly related to objectives 1 and 2 of our production system.

As related to objective 1, the expensive computation required for topography displacement will be performed only once, off-line. The obtained information will be saved into a file and utilized during on-line processing throughout the mission. This is possible due to the small orbit to orbit variations at the same location within an orbit path.

In regards to objective 2, we use unresempled but geolocated MISR imagery as the ground control information. The idea is that only MISR imagery with the same viewing geometry will provide a high success rate during least-square area based image matching.

As already mentioned, the ancillary dataset consists of two parts: a) Projection Parameters (PP) file, and b) Reference Orbit Imagery (ROI). The ROI consists of selected (cloud free) unresampled MISR imagery for which a set of PP is produced off-line using rigorous photogrammetric reduction methods. The PP file provides geolocation information for acquired MISR imagery on a pixel by pixel basis. This geolocation information is referenced to a selected Space Oblique Mercator map projection grid. The process of creating ROI and PP files is similar to the regular orthorectification of time dependent sensor imagery. The major differences are: a) acquired imagery is geolocated but not resampled, and b) a global DEM of sufficient resolution is available for MISR's internal use. In particular, a simultaneous bundle adjustment utilizing multi-angle imagery and ground control information (global DEM and ground control point chips) is used to model errors in the navigation and attitude data for a single set of ROI, prior to geolocation. The detailed description of the work involved in the creation of the ancillary dataset may be the subject of another article.

4.3 Image Point Intersection (IPI)

A rigorous ground-to-image projection (Paderes, 1989) is used to compute image coordinates of the initial tie points prior to image matching. It utilizes a well known collinearity condition modified for MISR time dependent imagery constrained by the equation which describes the spacecraft trajectory. It is obtained utilizing the ground point coordinates X, the position of the sensor at time of imaging P, and the pointing direction of the ray imaging the ground point, see

equation (1), all referenced to the Geocentric coordinate system:

$$X = P + \lambda \rho \qquad (2)$$

where λ is a scale factor. Using an iterative root-finding method, equation (2) can be solved for the image coordinate of the ground point. Initial input to the iterative solution is obtained from the ancillary dataset in conjuction with nominal orbit parameters.

4.4 Image Matching

An image matching technique has been chosen in order to: a) precisely locate tie points during image-to-image registration, and b) to estimate accuracy of the local image-to-image transformation (Ackermann, 1984). Our decision to use a combination of cross-correlation and least-square area based image matching method is based largely on two factors. First, the high subpixel accuracy of successful matches that can be achieved (Forstner, 1980). Second, MISR new and reference images with their minimal perspective changes between the two views will serve as very good input to the selected method. The size of the "target" and "search" windows are based on the expected errors in the supplied navigation and attitude data.

4.5 Image-to-Image Transformation

The form of the image-to-image transformation was derived by looking at the physical characteristics of a push broom camera. We built a model that describes how a scan line of the reference image maps to the new image. We then assumed that the mapping for nearby scan lines should be nearly identical. Although the model was derived for a single scan line, we apply it to a larger area (nominally 256 lines of data).

The physical aspects that were included are a) linear optics, b) earth curvature, and c) effect of ground topography.

If we ignore for a moment the effect of (b) and (c), then we have the situation pictured in Figure 5. In this approximation, all the look vectors for a single scan line lie in a plane. The ground is plane, so the intersection of the scan plane with the surface is a straight line. This is true for both the reference and the new image. This means that lines in the reference image get mapped to lines in the new image. The most general transformation that takes a line to a line is:

$$s_{new} = k_1 (l_{ref} - l_0) + k_2 (s_{ref} - s_0) + k_3 \qquad (3)$$

$$l_{new} = k_4 (l_{ref} - l_0) + k_5 (s_{ref} - s_0) + k_6 \qquad (4)$$

This is simply the affine model. l_0 and s_0 are the coordinates of the center of the line, e.g. l_0 is l_{ref} and s_0 is $1503 / 2 = 751.5$.

179

International Archives of Photogrammetry and Remote Sensing. Vol. XXXI, Part B2. Vienna 1996
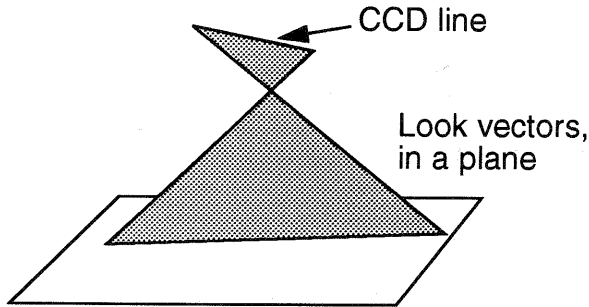
Figure 5: Scan line

We can include (b), the effect of the earth's curvature, by looking at the disparity between the new and reference image due to topography. Looking at Figure 6, we see that
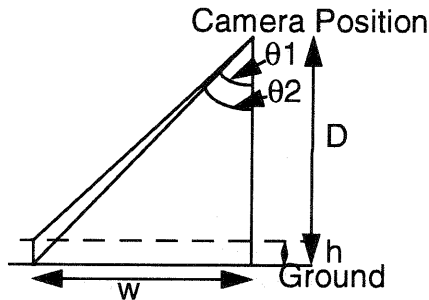

Figure 6: Finding effect of height change

$$\tan\theta_1 = \frac{w}{D} \tag{5}$$

$$\theta_2 - \theta_1 = \frac{w}{D^2 - w^2}h + O\left(\frac{wh^2}{D^3}\right) \tag{6}$$

In the linear optic approximation, we have

$$\theta = \theta_0 + \frac{(s - s_0)}{f}p \tag{7}$$

Where f is the focal length and p is the pitch. Using (7) and (6) we have

$$\Delta s_{new} - \Delta s_{ref} = \frac{p}{f}\left(\frac{w_{new}}{D_{new}^2 - w_{new}^2} - \frac{w_{ref}}{D_{ref}^2 - w_{ref}^2}\right)h \tag{8}$$

For a spherical model of the earth, simple geometry gives:

$$h = \sqrt{R_{earth}^2 - w_{new}^2} - h_0 \tag{9}$$

If we plug (7) into (5), then (5) into (9) and (8), and finally (9) into (8), we get an expression for $\Delta s_{new} - \Delta s_{ref}$ in terms of s_{new} and s_{ref}. We can then do a series expansion, to get an expression of the form:

$$\Delta s_{new} - \Delta s_{ref} = k_7 + k_8 s_{new} + k_9 s_{ref} + k_{10} s_{new}^2$$
$$+ k_{11} s_{ref} s_{new} + k_{12} s_{ref}^2 + \text{Higher Order} \tag{10}$$

The explicit form of the constant terms can be calculated, but they are unimportant for our use. What is important is that the quadratic coefficients are not zero, and that if we calculate the next order term we find that it is less than 10% of the quadratic terms.

Using a similar argument, we see that we can include (c), the effect of ground topography, by adding a term proportional to $h_{surface}$.

This gives a modification to (3) and (4) of

$$s_{new} = k_{14}(l_{ref} - l_0) + k_{15}(s_{ref} - s_0) + k_{16}(s_{ref} - s_0)^2 \tag{11}$$
$$+ k_{17}h_{surface} + k_{18}$$

$$l_{new} = k_{19}(l_{ref} - l_0) + k_{20}(s_{ref} - s_0) + k_{21}(s_{ref} - s_0)^2 \tag{12}$$
$$+ k_{22}h_{surface} + k_{23}$$

Testing shows that the corrections we have derived to the affine model are important. The quadratic term at the edges of the swath can be as large as 2 pixels. However, the height term is usually small, and in the Beta version of the MISR software it was dropped from the model.

We use this transform in the following manner:

1. Start with a region of imagery (nominally 256 lines, full swath).
2. Find well distributed conjugate points in the reference and new imagery. This requires finding points in areas where image matching can be performed (e.g., cloud free land).
3. Use the conjugate points to determine the coefficients in (11) and (12) by doing a least squares fit.
4. Find another set of conjugate points to use as check points. Compare the prediction of the location of the conjugate points in the new image by (11) and (12) to the actual location. If they are within the allowed tolerances (e.g., 1/2 pixel), then we are done. Otherwise, break the region into two smaller pieces, and repeat the process for each of the smaller pieces.

180

International Archives of Photogrammetry and Remote Sensing. Vol. XXXI, Part B2. Vienna 1996

Blunder Detection: A blunder detection function was implemented to prevent low accuracy and extra sub-girding effort caused by the appearance of blunders from image matching. The reliability of the image-to-image transformation was studied by examining the behavior of the cofactor matrix Q_{vv} of the residuals. The distribution of the control points are configured accordingly. Blunders are detected using a data snooping method by a combined test to the standardized residuals $\bar{v}_i$ and to the variance per unit weight σ_0.

Reduced Number of Tie Points: As described previously, the tie points coordinates are obtained using an image matching technique in addition to the supplied navigation and attitude data. However, ceratin conditions (e.g. deserts, cloud cover) in a MISR image will not allow for successful matching in those region. In those cases the corrections to the supplied navigation and attitude data are modeled as slowly varying parameters. These parameters are obtained through the use of a Kalman filter based on the information from the tie points previously matched.

Band-to-Band Transformation: The registration between the new MISR image and ROI imagery has been done using the red spectral band (Figure 3) because of its characteristics relative to the image matching requirements. The imagery from the other three bands will be registered to the already registered and geolocated red band. This registration does not include image matching. Rather, the transformation between bands is defined by the interior orientation parameters of the geometric camera model. More details on this transformation may be presented in a subsequent paper.

5. PROTOTYPE TESTING

Delivery of the beta version of the production software was in March of 1996, following an extensive prototype and testing phase. Landsat TM images and associated DEM have been used to produce simulated MISR data, and navigation and attitude data errors are included (Lewicki, 1994). Several test cases have been made with two objectives: 1) to represent a realistic range of perturbations and errors in the navigation and attitude data, and 2) to represent various cases in regards to the availability of a region suitable for image matching. Only in the worst combination of these factors (i.e. worst possible errors in the attitude, less then 50% of a region suitable for matching, and no information from the previous matching available) does our algorithm not meet geolocation accuracy requirements, which is not surprising. Otherwise, testing has demonstrated that georectification of MISR imagery which meets science accuracy requirements is feasible in an autonomous and continuous process.

6. ACKNOWLEDGMENTS

7. REFERENCES

[1]   Ackermann, F., Digital Image Correlation: Performance and Potential Application in Photogrammetry, Photogrammetric Record, vol. 11(64), 1984.

[2]   Diner, D. J., Bruegge, C. J., Martonchick, J. V., Bothwell, G. W., Danielson, E. D., Floyd, E. L., Ford, V. G., Hovland, L. E., Jones, K. L., and White, M. L., A Multiangle Imaging SpectroRadiometer for Terrestrial Remote Sensing from the Earth Observing System, International Journal of Imaging Systems and Technology, vol. 3, 1991.

[3]   Herrick, S,. Astrodynamics, Van Nostrand Reinhold, New York, 1971.

[4]   Forstner, W., On the Geometric Precision of Digital Correlation, ISPRS Int. Arch. of Photogrammetry, vol. XXIV, Commission III, Helsinki, 1980.

[5]   Lewicki, S. A., Smyth, M. M., Jovanovic, V. M., and Hansen, E. G., A Simulation of EOS MISR Data and Geometric Processing for the Prototyping of the MISR Ground Data System, IGARSS Proceedings, vol (3), 1994.

[6]   Mikhail, E. M., Observations and Least Square, Harper & Row, New York, 1976.

[7]   Paderes, F. C., Mikhail, E. M., and Fagerman, J. A., Batch and On-Line Evaluation of Stereo Spot Imagery, ASPRS Proceedings, vol. (3), 1989.

[8]   Snyder, J. P., Map Projection - A Working Manual, United States Geological Survey Professional Paper 1395, U. S. Government Printing Office, Washington, 1987.

181

International Archives of Photogrammetry and Remote Sensing. Vol. XXXI, Part B2. Vienna 1996